KCNQ1 and KCNE1 in the I_{Ks} Channel Complex Make State-dependent Contacts in their Extracellular Domains

Xulin Xu, Min Jiang, Kai-Ling Hsu, Mei Zhang, and Gea-Ny Tseng

Department of Physiology and Biophysics, Medical College of Virginia, Virginia Commonwealth University, Richmond, VA 23298

KCNQ1 and KCNE1 (Q1 and E1) associate to form the slow delayed rectifier I_{Ks} channels in the heart. A short stretch of eight amino acids at the extracellular end of S1 in Q1 (positions 140–147) harbors six arrhythmia-associated mutations. Some of these mutations affect the Q1 channel function only when coexpressed with E1, suggesting that this Q1 region may engage in the interaction with E1 critical for the I_{Ks} channel function. Identifying the Q1/E1 contact points here may provide new insights into how the I_{Ks} channel operates. We focus on Q1 position 145 and E1 positions 40–43. Replacing all native cysteine (Cys) in Q1 and introducing Cys into the above Q1 and E1 positions do not significantly perturb the Q1 channel function or Q1/E1 interactions. Immunoblot experiments on COS-7 cells reveal that Q1 145C can form disulfide bonds with E1 40C and 41C, but not E1 42C or 43C. Correspondingly, voltage clamp experiments in oocytes reveal that Q1 145C coexpressed with E1 40C or E1 41C manifests unique gating behavior and DTT sensitivity. Our data suggest that E1 40C and 41C come close to Q1 145C in the activated and resting states, respectively, to allow disulfide bond formation. These data and those in the literature lead us to propose a structural model for the Q1/E1 channel complex, in which E1 is located between S1, S4, and S6 of three separate Q1 subunits. We propose that E1 is not a passive partner of the Q1 channel, but instead can engage in molecular motions during I_{Ks} gating.

The Journal of General Physiology

INTRODUCTION

The slow delayed rectifier (I_{Ks}) channel is expressed in human heart and contributes to action potential repolarization (Wang et al., 1994; Li et al., 1996; Jost et al., 2005). The I_{Ks} channel has at least two components: a major pore-forming component (KCNQ1 channel, also known as Kv7.1 or KvLQT1, abbreviated as Q1 in the following text) and a small auxiliary component (KCNE1, also known as minK or IsK, abbreviated as E1) (Barhanin et al., 1996; Sanguinetti et al., 1996). Q1 is a typical voltage-gated (Kv) channel. Each channel has four subunits and each subunit consists of six transmembrane segments (S1–S6) and a reentrant pore-lining loop (P-loop) (2-D diagram of a Q1 subunit in Fig. 1). Based on the crystal structure of Kv1.2 (Long et al., 2005a), S1–S4 form the peripheral voltage-sensing domain (VSD), and S5-P loop-S6 form the central pore domain (PD). When Q1 is expressed alone, it mediates a relatively fast-activating, slowly deactivating K current (Barhanin et al., 1996; Sanguinetti et al., 1996). It also exhibits a fast, nonabsorbing inactivation gating process (Tristani-Firouzi and Sanguinetti, 1998). There has been no sighting of lone Q1 currents in cardiac myocytes. Instead, Q1 appears to exit mostly in Q1/E1 channel complexes, although additional or separate associations with KCNE2 (Wu et al., 2006a) and other KCNE subunits (Morin and Kobertz, 2007) are possible.

E1 is the founding member of the KCNE family of voltage-gated channel auxiliary subunits (Abbott and Goldstein, 1998). There are five members in this family: KCNE1–KCNE5. These are single membrane-spanning proteins with amino and carboxyl termini in the extracellular and intracellular compartments, respectively (2-D diagram of E1, Fig. 1). E1 association induces the following changes in the Q1 channel function: (1) increase in single channel conductance and thus a larger macroscopic current amplitude (Sesti and Goldstein, 1998), (2) slowing of activation and positive shift in the voltage dependence of activation (Barhanin et al., 1996; Sanguinetti et al., 1996), and (3) suppression of inactivation (Tristani-Firouzi and Sanguinetti, 1998). There has been a long quest for the structural basis and mechanism of E1 modulation of Q1. Previous studies have shown that the transmembrane domain (TMD) of E1 mediates association with the Q1 channel (Tapper and George, 2000; Chen and Goldstein, 2007). NMR spectroscopy and scanning mutagenesis experiments have indicated that the TMD of E1 (aa 44–67) adopts an α-helical structure (Aggeli et al., 1998; Chen and Goldstein, 2007; Tian et al., 2007). It has been suggested that the TMD of E1 interacts with the pore domain of Q1, and in particular, the S6 segment (region of identified interactions, Fig. 1) (Goldstein and Miller, 1991; Tai and Goldstein, 1998; Tapper and George, 2001;

Correspondence to Gea-Ny Tseng: gtseng@vcu.edu

The online version of this article contains supplemental material.

Abbreviations used in this paper: NEM, *N*-ethylmaleimide; PD, pore domain; TMD, transmembrane domain; VSD, voltage-sensing domain.

The Rockefeller University Press $30.00
J. Gen. Physiol. Vol. 131 No. 6 589–603
www.jgp.org/cgi/doi/10.1085/jgp.200809976

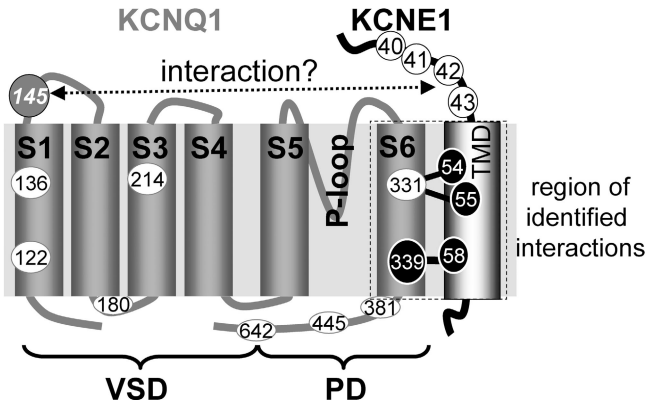

Figure 1. 2-D diagram of KCNQ1 and KCNE1 subunits. For Q1, transmembrane segments S1–S6, P-loop, voltage-sensing domain (VSD), and pore-domain (PD) are marked. Numbers in ovals denote positions of native cysteine (Cys) in Q1 that have been replaced by Ala in the Q1(-Cys)-WT construct. Ile at position 145 is replaced by Cys to create the Q1(-Cys)-I145C construct. Region of interactions identified in previous studies is outlined by a dotted rectangle, and specific interacting residues are linked by solid lines (Tapper and George, 2001; Melman et al., 2002; Panaghie et al., 2006). Potential interaction between the extracellular end of Q1 S1 and the extracellular end of E1 transmembrane domain (TMD) investigated in this study is denoted by a dotted line.

Melman et al., 2004; Panaghie et al., 2006). This is consistent with the structural role of S6 in Kv channels: lining the inner cavity and harboring the activation gate (Liu and Joho, 1998; Hackos et al., 2002). However, recent data suggest that E1 can also interact with the VSD of Q1. For example, it has been suggested that E1 modulation of Q1 gating kinetics critically depends on the charge distribution pattern in the carboxyl half of Q1's S4 (Panaghie and Abbott, 2007). Furthermore, the extracellular end of E1 TMD can come very close to the extracellular end of S4 in Q1, so that two cysteine side chains engineered here (at E1 position 43 and Q1 position 226) can form a disulfide bond across the Q1/E1 interface (Nakajo and Kubo, 2007).

In this study, we focus on the extracellular end of S1 in Q1 (position 145). Our interest in this region of Q1 stems from the observations that a short stretch of amino acids here (positions 140–147) harbors six arrhythmia-associated mutations (Chen et al., 2003b; Zareba et al., 2003; Hong et al., 2005; Napolitano et al., 2005; Liu et al., 2006; Lundby et al., 2007). Furthermore, for at least three of them, the manifestation of the abnormal phenotypes requires E1 coexpression. When S140G, V141M, or Q147R is expressed alone, the channel behaves like wild-type (WT) Q1, indicating that the mutations per se do not perturb the Q1 channel function (Chen et al., 2003b; Hong et al., 2005; Lundby et al., 2007). However, when these Q1 mutants are coexpressed with E1, the mutant Q1/E1 channel complexes either become constitutively active (S140G and V141M, gain-of-function mutations) (Chen et al., 2003b; Hong et al., 2005) or have reduced current amplitude (Q147R, loss-of-function mutation) (Lundby et al., 2007). These observations suggest that the extracellular end of S1 in Q1 is involved in Q1/E1 interactions, which impact on the channel gating kinetics and current amplitude. We focus on the extracellular end of E1 TMD (positions 40–43) as a potential region engaged in interactions with Q1. It has been suggested that this region of E1 is involved in the binding and/or action of I_{Ks} activators of the stilbene and fenamate types (Abitbol et al., 1999). These I_{Ks} activators work from outside the cell membrane by shifting the voltage dependence of Q1 activation in the negative direction. The degree of shift is enhanced by E1 association (Wu et al., 2006b). Mutations or deletions in the 39–42 region of E1 abolish these activators' actions (Abitbol et al., 1999). Therefore, this region of E1 may be involved in interaction with Q1 that impacts on the activation gating process of the Q1/E1 channel complex.

We use the approach of "disulfide trapping" to probe the relationship between Q1 position 145 and E1 positions 40–43. To form a disulfide bond, two thiol side chains need to come close to each other so that the distance between their C_β atoms (C_β–C_β distance) reaches ~4.6 Å (Careaga and Falke, 1992). This can occur between thiol side chains as far apart as 15 Å, if they are in flexible regions of proteins. The rate of disulfide bond formation reduces as the C_β–C_β distance lengthens (Careaga and Falke, 1992). Therefore, the degree and rate of disulfide bond formation can be used to deduce the distance between thiol side chains and peptide backbone flexibility. To avoid interference in data interpretation, we replace all the Q1 native Cys with Ala to create a Cys-less Q1 background, and then introduce Cys into position 145 (Fig. 1). There is one native Cys in E1 (position 102, in the cytoplasmic domain). C102 should not interfere with data interpretation, because we aim to detect disulfide bond formation when the channel complexes are embedded in membrane lipid bilayer, and C102 is not accessible to the extracellular Q1 position. We use COS-7 expression and immunoblotting to probe for disulfide bond formation between engineered Cys side chains, one on Q1 and the other on E1. We then use voltage clamp experiments in oocytes to probe for functional consequences, as well as the state dependence and rate of disulfide bond formation.

MATERIALS AND METHODS

Molecular Biology and Side-directed Mutagenesis

Human Q1 and E1 cDNAs are generous gifts from M.T. Keating (Harvard University, Cambridge, MA) and R. Swanson (Merck Company, West Point, PA). Six Q1 splice variants (isoforms 0–5) have been reported (Jespersen et al., 2005). We use isoform 0 (Sanguinetti et al., 1996) in the current study. Relative to isoform

1, isoform 0 has a shorter cytoplasmic amino-terminal domain and is expressed more consistently in oocytes. Isoform 0 exhibits the same gating properties and the same pattern of modulation by KCNE subunits as isoform 1 (Wu et al., 2006a). For comparison with the literature, we use the numbering of isoform 1 to specify Q1 positions where native Cys have been removed (eight in total) and where cysteine substitution is made (Fig. 1). Q1 is subcloned into vector pcDNA3.1/V5-His-TOPO (Invitrogen, for COS-7 expression) or pSP64 (Promega, for oocyte expression). E1 and E2 are subcloned into pAlterMax (Promega, COS-7 and oocyte expression). Mutations are created using the QuickChange mutagenesis kit (Invitrogen) and confirmed by direct DNA sequencing. The Q1 variants are named as Q1-WT, Q1(-Cys)-WT, and Q1(-Cys)-I145C. The E1 variants are named as E1-WT and E1-AxxC (where A = native residue, xx = position number). For in vitro transcription, plasmids are linearized by a suitable restriction enzyme and transcribed using SP6 or T7 RNA polymerase and commercial kits (Mmessage Mmachine, Ambion). The cRNA products are run on denaturing RNA gels and stained with ethidium bromide. The cRNA band sizes and intensities are quantified by densitometry (ChemiImager model 4400, Alpha-Innotech Corp.), using a known amount of RNA size markers as reference.

Oocyte Expression and "2-Cushion Pipette" Voltage Clamp Recording

Oocytes are isolated as described before (Tseng-Crank et al., 1990) and incubated in an ND96-based medium (composition given below), supplemented with 4% horse serum and penicillin/streptomycin at 16°C. 2–14 h after isolation, oocytes are injected with cRNA(s) using a Drummond digital microdispenser. Each oocyte receives 10 ng of Q1 cRNA and/or 3 ng of E1 cRNA (molar ratio of Q1: E1 = 1:1). The most important advantage of the oocyte expression system is that it allows us to control the amounts of cRNA injected, so that we have better control of the expression level of Q1 and E1 subunits. However, oocytes express an endogenous Q1 subunit, xQ1 (Sanguinetti et al., 1996) that can potentially interfere with data interpretation. We use the following strategies to guard against this artifact: (a) keep the amount of injected E1 cRNA low (3 ng/oocyte), (b) always prepare oocytes injected with E1-WT cRNA alone to check xQ1 interference (and use frogs whose oocytes express little or no I_{Ks} when injected with E1-WT cRNA alone, Fig. 2), and (c) record currents 4–5 d after cRNA injection, when oocytes injected with E1-WT alone have little or no I_{Ks}-like currents. Fig. 2 shows typical results from one such experiment.

In some oocytes depolarization pulses to above +80 mV induce a transient inward current (upon repolarization to −60 mV) superimposed on the outward tail current through the Q1 or Q1/E1 channels. This transient inward current is likely due to a combination of transient extracellular K^+ ion accumulation in oocyte cell membrane invaginations and a time-dependent endogenous Cl^- current. Whether we accept data from these oocytes is determined during off-line data analysis. If the absolute peak amplitude of such transient inward current is estimated to be ~20% or less of the projected peak amplitude of outward tail current mediated by the Q1 or Q1/E1 channels after a test pulse to +80 mV, we accept the data but move the cursor to a later time point (after the decay of the transient inward current) for tail current amplitude measurement. Assuming that the tail currents of the Q1 or Q1/E1 channel complex deactivate with the same time course following depolarizations to different voltages, we believe such a measurement can give a faithful quantification of the degree of channel activation by the depolarizing pulses. If the interference by the transient inward current is judged to be more severe, data from the oocyte are discarded.

Whole oocyte membrane currents are recorded using the "2-cushion pipette" voltage clamp method (Schreibmayer et al., 1994).

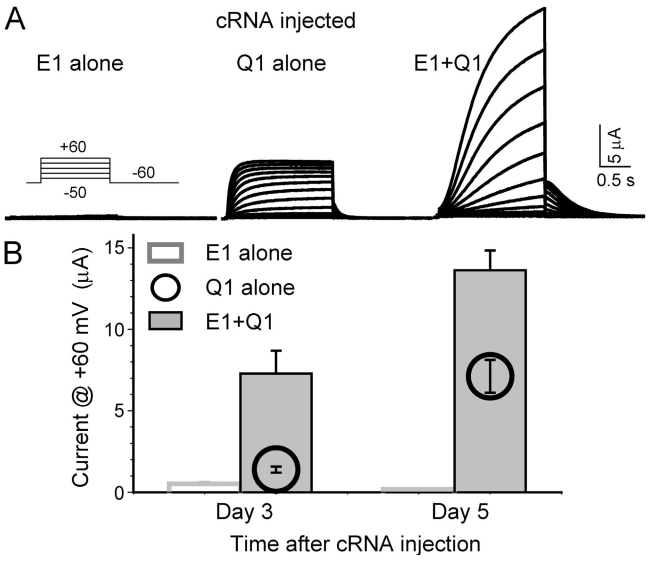

Figure 2. Validating the oocyte expression system for study of Q1/E1 interaction. Each oocyte is injected with cRNA for E1-WT alone (3 ng/oocyte, to monitor currents through oocyte endogenous xQ1 associated with E1-WT) (Sanguinetti et al., 1996), Q1-WT alone (10 ng/oocyte), or Q1-WT + E1-WT (10 and 3 ng per oocyte, respectively, cRNA molar ratio 1:1). Membrane currents are recorded on days 3 and 5 after cRNA injection. (A) Representative current traces elicited by the diagrammed protocol from oocytes injected with marked cRNA(s). (B) Mean current amplitudes at +60 mV from the three groups of oocytes. Note that the E1-alone currents are almost invisible at the same gain suitable for the other two groups, and the SE bar is buried in the line of the histogram bars. In all the experiments reported in this study, we inject the same amount of cRNA for Q1 and/or E1 variant per oocyte as listed above, including E1-WT alone, and currents are recorded on days 4–5 (unless otherwise noted). To quantify and compare current amplitudes in oocytes expressing Q1 plus E1 vs. Q1 alone, data from the former group are corrected for mean current amplitude of oocytes injected with E1-WT alone (representing contribution from oocyte xQ1/E1-WT in the same batch of oocytes).

Both current-passing and voltage-recording pipettes have a low tip resistance of 0.1–0.3 MΩ, to achieve a fast speed of voltage clamping. During recording, the oocyte is continuously superfused with a low-Cl ND96 solution to reduce interference from endogenous Cl channels. We use 3 M KCl (in 1% agarose) salt bridges to connect the bath solution to Ag/AgCl pellets in the reference half-cells, thus avoiding liquid junction and liquid-metal surface potentials in our recording system. Voltage clamp is done at room temperature (24–26°C) with OC-725B or OC-725C amplifier (Warner Instruments). Voltage clamp protocol generation and data acquisition are controlled by pClamp 5.5 via a 12-bit D/A and A/D converter (DMA, Axon Instruments). Current data are low-pass filtered at 1 kHz (Frequency Devices) and stored on disks for off-line analysis. The voltage clamp protocols and methods of data analysis are described in figure legends and text. The following software is used for data analysis: pClamp 6 or 10, EXCEL (Microsoft), SigmaPlot, SigmaStat, and PeakFit (SPSS).

The following solutions are used: (a) ND96 solution (in mM): NaCl 96, KCl 2, $CaCl_2$ 1.8, $MgCl_2$ 1, HEPES 5, Na-pyruvate 2.5, pH 7.5, and (b) low-Cl ND96: Cl^- ions in ND96 replaced by methanesulfonate. HMR 1556 (Aventis Pharma Deutschland GmbH) is dissolved in DMSO at 10 mM, and added to the bath solution before experiments to reach the final concentration (10 μM).

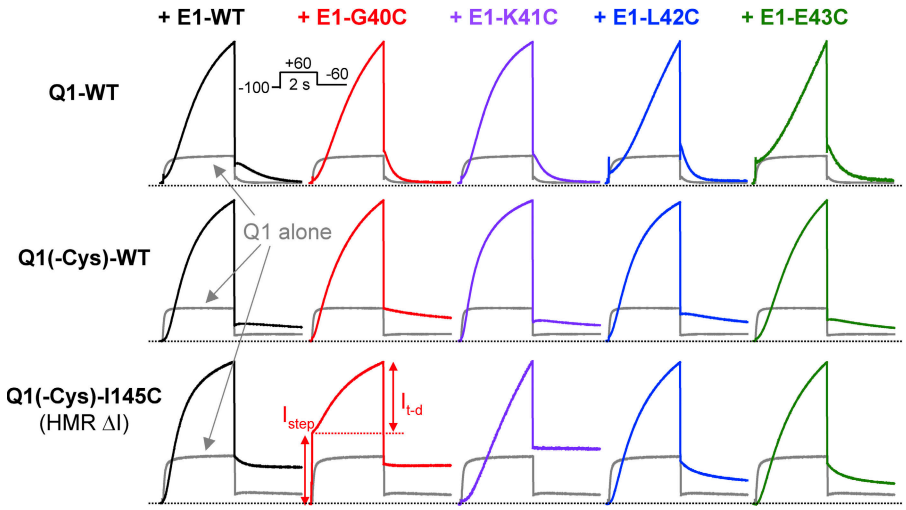

Figure 3. Q1 and E1 mutations investigated in this study preserve Q1 channel function and Q1/E1 interactions. Current traces are recorded from three batches of oocytes, expressing Q1-WT (top), Q1(-Cys)-WT (middle), or Q1(-Cys)-I145C (bottom), alone or with E1 WT or mutants at 1:1 cRNA molar ratio. The type of Q1 variant is marked on the left of each row, while the type of E1 variant is marked on the top of each column. In the case of Q1(-Cys)-I145C coexpressed with Cys-substituted E1 mutants, oocytes are treated with DTT (10 mM for 10 min, or 25 mM for 5 min) and thoroughly rinsed before current recording. The voltage clamp protocol is diagrammed in the inset of top row. To illustrate the effects of E1 variants on the channel function of each of the Q1 variants, in each row the same representative current trace recorded from an oocyte expressing respective Q1 variant alone is shown as a gray trace, superimposed with current traces from oocytes coexpressing E1 variants. To illustrate the current enhancing effects of E1 variants on the Q1 channels, the current traces are scaled to reflect the average ratio of current amplitudes of Q1+E1 vs. Q1 alone in the same batch of oocytes (the exact numbers of fold-increase in current amplitudes are listed in Table II). Q1(-Cys)-I145C coexpressed with E1-G40C manifests a unique time-independent component (I_{step}) and a time-dependent component ($I_{t\text{-}d}$). To ascertain that this is not due to interference from oocyte leak conductance, current traces in the third row are HMR-sensitive current (HMR ΔI = control current – current recorded in the presence of 10 uM HMR; Wu et al., 2006a). Dotted lines denote the zero current level.

COS-7 Expression and Western Blotting

COS-7 cells are maintained in D-MEM (GIBCO BRL) supplemented with 10% FCS (Hyclone) and penicillin/streptomycin, in a moist 5% CO_2 chamber at 36°C. Cells are plated at a subconfluence level the day before transfection. In most experiments, the following amounts of cDNA are added to each 35-mm dish: Q1 = 2 μg, E1 = 2.8 μg (molar ratio Q1:E1 = 1:2). In a pilot experiment, changing the Q1(-Cys)-I145C and E1-G40C cDNA molar ratio (1:0.5, 1:1, and 1:2) does not affect the immunoblot results.

COS-7 cells are scraped off Petri dishes and incubated in 20 mM *N*-ethylmaleimide (NEM) on ice for 10 min before making whole cell lysate. The NEM treatment protects free thiol groups from forming nonnative disulfide bonds after channel proteins are released from their cell membrane confinement. Unless otherwise stated, all the following procedures are conducted in nonreducing conditions at 4°C or on ice, in the presence of a cocktail of protease inhibitors. Cells are lysed by repeated freeze/thawing cycles in a lysis buffer (3% SDS, 10% glycerol, 62.5 mM Tris-HCl, 1 mM EDTA, pH 6.8). After low-speed centrifugation, the postnuclear supernatants are collected for immunoblotting. In some experiments, cells or protein samples are treated with DTT (10 mM, 10 min, room temperature) to break disulfide bonds. Protein samples are loaded onto 7.5% (for Q1 immunoblots) or 14% (for E1 immunoblots) nonreducing SDS polyacrylamide gels. After fractionation, the proteins are blotted onto PVDF membranes (Amersham Biosciences), and probed for Q1 (V5 mAb from Invitrogen, or Q1 pAb from Santa Cruz Biotechnology, Inc.) or E1 pAb (Alomone). Immunoreactivity is visualized using an ECL detection kit (Amersham), and band intensities are quantified by densitometry (ChemiImager model 4400).

Immunoprecipitation and Enzyme Deglycosylation Experiments

COS-7 cells transfected with various cDNA(s) or mock transfected (as negative control) are NEM-treated and lysed in the same buffer as described above, except that the samples are heated to 60°C for 2 min to promote dissociation of noncovalently associated Q1 and E1 but not disulfide-linked Q1/E1. After preclearing with protein G beads, the whole cell lysates are subjected to immunoprecipitation with V5-mAb. Immunoprecipitated Q1 along with disulfide linked E1, if present, is eluted using SDS-PAGE sample buffer that contains 5 mM DTT to release the disulfide linked E1. Immunoprecipitates and the original whole cell lysates (direct input) are loaded onto 4–20% gradient nonreducing gel and fractionated by electrophoresis. After blotting the proteins to a PVDF membrane, the upper portion of the membrane (above the 37-kD size marker band) is probed for Q1 using C-20 pAb, and the lower portion is probed for E1 using the Alomone pAb.

Whole cell lysate from COS-7 cells transfected with Q1(-Cys)-I145C and E1-G40C is divided into four aliquots. Two are treated with PNGase F (Sigma-Aldrich, 10 U/200 μg protein) under nonreducing conditions in the presence of a cocktail of protease inhibitors at 37°C for 24 or 48 h, and the other two aliquots are incubated under the same conditions for 24 or 48 h without PNGase F. We use such long incubation times as a precaution to ensure as complete deglycosylation of the Q1 and E1 proteins as possible. This is because we do not include any reducing agent in the buffer as recommended by the manufacturer, and the PNGase F enzymatic activity is expected to be low. All four aliquots are fractionated by 4–20% gradient nonreducing SDS-PAGE, blotted to PVDF membrane, and probed for Q1 and E1 immunoreactive bands as described above.

Online Supplemental Material

The online supplemental material (Fig. S1) is available at http://www.jgp.org/cgi/content/full/jgp.200809976/DC1. Q1 subcloned into vector pcDNA3.1/V5-His-TOPO (used for COS-7 expression) has inframe V5 (GKPIPNPLLGLDST) and His (HHHHHH) epitope tags attached to the carboxyl terminus. We use the oocyte expression system to test whether epitope tagging perturbs Q1 channel function or Q1/E1 interaction. Because cRNAs made from the TOPO vector do not have a poly(A) tail, their expression efficiency in oocytes is low. Therefore, we increase the Q1 cRNA to 25 ng/oocyte and the E1 cRNA to 10 ng/oocyte, keeping the cRNA molar ratio of Q1:E1 at 1:1. Furthermore, to distinguish currents mediated by exogenous Q1 channels from

TABLE I

Activation Gating Parameters for KCNQ1 Variants Expressed Alone or with KCNE1 Variants

Subunit composition	$V_{0.5}$ (mV)	z_g	Constitutive component (%)	*n*
Q1-WT alone	−22.3 ± 1.2	3.28 ± 0.08	0	15
+ E1-WT	20.5 ± 2.4	1.82 ± 0.06	0	18
+ E1-G40C	16.4 ± 1.3	1.96 ± 0.06	0	16
+ E1-K41C	16.3 ± 1.9	1.84 ± 0.07	0	18
+ E1-L42C	49.9 ± 2.4	1.53 ± 0.05	0	18
+ E1-E43C	63.1 ± 2.1	1.40 ± 0.01	0	3
Q1(-Cys)-WT alone	−54.2 ± 0.6	3.87 ± 0.12	0	21
+ E1-WT	−14.1 ± 3.6	2.11 ± 0.09	0	9
+ E1-G40C	−6.3 ± 3.4	1.54 ± 0.04	0	13
+ E1-K41C	−21.9 ± 4.9	1.80 ± 0.11	0	9
+ E1-L42C	−12.7 ± 1.4	1.54 ± 0.08	0	10
+ E1-E43C	14.7 ± 4.5	1.58 ± 0.06	0	6
Q1(-Cys)-I145C	−55.2 ± 0.6	3.58 ± 0.07	0	19
+ E1-WT	−14.1 ± 5.8	1.19 ± 0.07	0	6
+ E1- WT (after DTT)	−20.1 ± 5.5	0.97 ± 0.09	0	3
+ E1-G40C	32.3 ± 4.0	0.88 ± 0.05	0	8
+ E1-G40C (after DTT)	2.1 ± 6.3	0.95 ± 0.11	42.3 ± 7.3	8
+ E1-K41C	80.2 ± 5.7	0.68 ± 0.02	0	9
+ E1-K41C (after DTT)	55.0 ± 5.8	0.82 ± 0.04	0	9
+ E1-L42C	2.0 ± 3.4	1.61 ± 0.11	0	5
+ E1-L42C (after DTT)	−2.7 ± 6.4	1.20 ± 0.05	0	5
+ E1-E43C	−2.4 ± 2.4	1.54 ± 0.09	0	4
+ E1-E43C (after DTT)	5.7 ± 1.8	1.19 ± 0.06	0	5

The following voltage clamp protocol is used: from V_h −100 mV, 2-s depolarizing test pulses to V_t of −50 to +100 mV in 10-mV increments are applied at an interpulse interval of 30 s. The test pulses are followed by a 2-s step to −60 mV, during which tail currents are measured. The relationship between V_t and peak amplitudes of tail currents (I_{tail}) is fit with a simple Boltzmann function (except DTT-treated Q1(-Cys)-I145C/E1-G40C): $I_{tail} = I_{max}/(1 + \exp[(z_g(V_{0.5} - V_t)F/RT])$, where I_{max} = estimated maximal I_{tail}, z_g = apparent gating charge, $V_{0.5}$ = half-maximum activation voltage, F = Faraday constant, R = gas constant, and T = absolute temperature. Currents from DTT-treated Q1(-Cys)-I145C/E1-G40C manifest a prominent constitutive component. In this case, the data are fit with a modified Boltzmann function: $I_{tail} = I_{tail,step} + I_{tail,t\text{-}d}/(1 + \exp[(z_g(V_{0.5} - V_t)F/RT])$, where $I_{tail,step}$ and $I_{tail,t\text{-}d}$ represent tail currents of the constitutive and time-dependent components, respectively. Data are pooled from two to four batches of oocytes (*n* = total number of oocytes studied). After DTT: oocytes are treated with DTT (10 mM for 10 min or 25 mM for 5 min at room temperature, followed by thorough rinsing) before voltage clamping.

oocyte endogenous currents, we use 10 uM HMR to block currents through channels mediated by exogenous Q1 channels. All oocytes expressing Q1(-Cys)-I145C and Cys-substituted E1 variants are DTT pretreated. The results show that the Q1(-Cys)-I145C channel function and modulation by E1 variants are the same either in the TOPO vector or the pSP64 vector.

RESULTS

Testing whether Mutations Created in this Study Perturb the KCNQ1 Channel Function or KCNQ1/KCNE1 Interactions

The Cys substitution and disulfide trapping strategy is a powerful approach to probe the structure and function relationships of proteins. Functional perturbation should occur after disulfide bond formation between the engineered Cys residues. One can then use the extent and/or rate of disulfide bond formation to infer proximity relationships between positions of interest, or flexibility of peptide backbone(s) harboring these positions. A prerequisite is that the introduced mutations per se should not grossly perturb the native conformations and the function of the proteins, so that the above information can be translated back to the native states of the proteins. In this study, we replace all native Cys in Q1 with Ala to create the Q1(-Cys)-WT background. We then replace Ile at position 145 with Cys to create Q1(-Cys)-I145C. Does substituting native Cys with Ala, and/or substituting Ile145 with Cys, disrupt the Q1 channel function or Q1 modulation by E1? We also introduce Cys into E1 positions 40–43. Do these mutations disrupt E1 function as a Q1 channel modulator? To address these questions, we express all three Q1 variants (Q1-WT, Q1(-Cys)-WT, and Q1(-Cys)-I145C) alone or with E1 variants (E1-WT, E1-G40C, E1-K41C, E1-L42C, and E1-E43C) in *Xenopus* oocytes, and examine their function using the 2-cushion pipette voltage clamp technique. When the Q1 variants are expressed alone, they exhibit voltage-gated channel function similar to each other (gray "Q1 alone" current traces shown in Fig. 3). The most noticeable difference between Q1-WT and Q1(-Cys)-WT is a slowing of deactivation in the latter

TABLE II

Degree of Increase in KCNQ1 Current Amplitude by KCNE1 WT and Mutants

	Q1 alone	+ E1-WT	+ E1-G40C	+ E1-K41C	+ E1-L42C	+ E1-E43C
Q1-WT						
Mean	1.00	2.67	2.77	2.39	1.25	0.38[a]
SEM	0.19	0.32	0.21	0.42	0.27	0.11
n	14	11	8	9	9	6
Q1(-Cys)-WT						
Mean	1.00	8.45	2.43	6.45	1.95	2.05
SEM	0.13	1.67	0.53	0.93	0.13	0.34
n	21	9	7	5	11	5
Q1(-Cys)-I145C						
Mean	1.00	4.51	11.00	3.39	4.19	3.52
SEM	0.32	0.49	2.13	0.52	0.80	0.69
n	14	11	8	8	11	9

Total current amplitudes in oocytes coexpressing E1 with Q1 are corrected for interference by *Xenopus* endogenous Q1 (estimated by the mean current amplitude from oocytes expressing E1-WT alone, n =14–21 per batch of oocytes). These current amplitudes, and the current amplitudes from oocytes expressing Q1 alone, are then corrected for differences in the degrees of activation at the test voltage when current amplitudes are measured (based on the average 2-s isochronal activation curves), and then normalized by the mean current from oocytes expressing Q1 alone.

[a]In multiple experiments, most oocytes expressing E1-E43C with Q1-WT die 2 d after cRNA injection. Therefore, the current amplitudes of Q1-WT/E1-E43C are limited to data obtained ~1 d after cRNA injection, earlier than data from the other groups of oocytes.

(Fig. 3, compare the "Q1 alone" traces between the first and second rows), in conjunction with a negative shift in its voltage dependence of activation (Table I). Therefore, replacing all native Cys in Q1 with Ala causes a stabilization of channels in the open versus closed states. Replacing Ile145 with Cys in the Q1(-Cys)-WT background does not induce further changes in the channel function (Fig. 3, "Q1 alone" traces between the second and third rows, and Table I).

To judge whether channel complexes composed of these Q1 and E1 variants maintain the native conformation and function of the WT Q1/E1 channel complex, we look for the hallmarks of Q1 modulation by E1: (a) increase in current amplitude, (b) slowing of activation, and (c) positive shift in the voltage range of activation. Fig. 3 illustrates current traces recorded from all the combinations of Q1/E1 variants superimposed on respective "Q1 alone" current traces. In the case of Q1(-Cys)-I145C coexpressed with Cys-substituted E1 mutants, all oocytes are DTT pretreated to reduce disulfide bonds before recording. However, disulfide bonds can reform between some of these Cys pairs after DTT removal (see below). Even with this caveat, for all the combinations of Q1/E1 complexes, the E1 variants consistently induce the following changes in Q1 variants: slowing activation (Fig. 3), positive shift in the voltage dependence of activation (Table I), and increase in current amplitude (Table II).

The Q1/E1 channel complexes containing Q1(-Cys)-WT or Q1(-Cys)-I145C deactivate very slowly (Fig. 3, second and third rows, tail currents do not totally decay to baseline by the end of 2-s repolarization to −60 mV). Because of the slow rates of deactivation, we use a hyperpolarized holding voltage (V_h, −100 mV) and a long interpulse interval (30 s) to ensure that channel deactivation is complete between pulses. Otherwise, incomplete channel deactivation between pulses will create an apparent "instantaneous current component" upon membrane depolarization. With this precaution, DTT-pretreated Q1(-Cys)-I145C/E1-G40C manifests a uniquely prominent instantaneous current component upon membrane depolarization (I_{Step}, Fig. 3). This instantaneous current component persists even at V_h −120 or −140 mV (unpublished data). It is not due to a nonspecific "leak" conductance of the oocyte cell membrane, because it can be suppressed by HMR1556 (which does not inhibit oocyte endogenous currents) (Wu et al., 2006a). In fact, the current traces shown in the third row of Fig. 3 are all HMR-sensitive currents. Even with this unique property, the Q1(-Cys)-I145C/E1-G40C channel complex exhibits the hallmarks of Q1 modulation by E1: relative to Q1(-Cys)-I145C alone, E1-G40C coexpression slows activation (considering the time-dependent component, $I_{t\text{-}d}$), shifts the voltage range of activation of $I_{t\text{-}d}$ in the positive direction (Table I), and markedly increases the current amplitude (Table II).

We conclude that in all the combinations of Q1/E1 variants, the Q1 channel function and Q1 modulation by E1 are preserved. These observations indicate that the mutant Q1/E1 pairs preserve the essential aspects of the native conformation in the WT Q1/E1 channel complex. Therefore, the information about Q1 and E1 interactions obtained from the following disulfide trapping experiments can be used to infer the proximity relationship and/or peptide backbone mobility in the native conformation of the Q1/E1 channel complex.

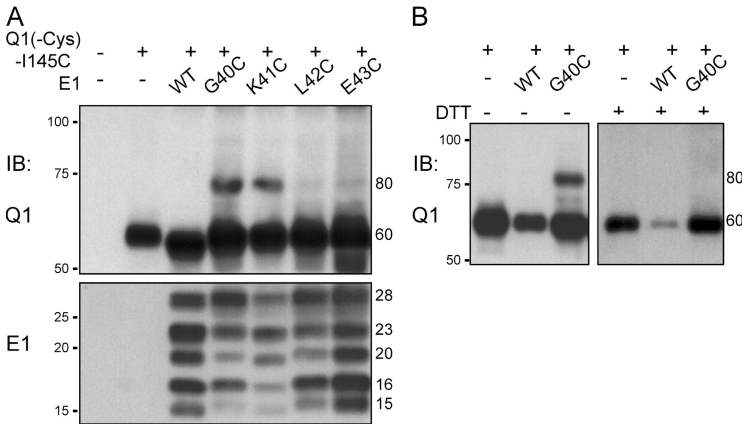

Figure 4. Testing disulfide bond formation between Q1 145C and Cys introduced into E1 positions 40–43. (A) COS-7 cells are transfected with cDNA(s) listed above (leftmost lane: no cDNA negative control). 48 h after transfection, cells are treated with NEM (to protect free thiol groups) followed by whole cell lysis and solubilization. Whole cell lysates are run on 7.5% and 14% nonreducing SDS gels. The former is probed for Q1 (with a V5 mAb targeting V5 epitope attached to the carboxyl end of Q1) and the latter is probed for E1 (with E1 pAb). Size marker positions are listed on the left, and sizes of Q1- or E1-specific bands are noted on the right (in kD). (B) Whole cell lysates prepared from COS-7 cells transfected with cDNA(s) listed above are each divided into two aliquots. One aliquot is treated with DTT (10 mM, room temperature, 10 min) while the other is incubated with buffer under the same conditions without DTT. All samples are run on a nonreducing SDS gel and probed for Q1 with V5 mAb.

Testing Disulfide Bond Formation between Q1 145C and E1 40C–43C

We use COS-7 cell expression and immunoblots to test disulfide bond formation between Q1 145C and E1 40C–43C. COS-7 cells provide the advantages of a high efficiency in protein expression and easiness in preparing whole cell lysate for immunoblot experiments (relative to oocytes). COS-7 cells are transfected with different combinations of Q1 and E1 variants and cultured for 48 h before experiments. To ensure that any disulfide bond formation detected in the Q1/E1 complexes occurs spontaneously (oxidized by ambient oxygen) when the channels are in their native conformation in the cell membrane, COS-7 cells are treated with NEM to covalently modify all remaining free thiol groups before making whole cell lysates. The following procedures are performed under nonreducing conditions to preserve disulfide bonds formed before the cell membrane is disrupted. A positive identification of disulfide bond formation between Q1 and E1 needs to satisfy the following criteria: (a) seen only when both Cys residues are present in the Q1/E1 complex, one on Q1 and the other on E1, but not when only one of the Cys residues is present (e.g., Q1(-Cys)-I145C coexpressed with E1-WT), (b) exhibiting a mobility in nonreducing gel expected for a 1:1 Q1/E1 complex, and (c) abolished if the cells or whole cell lysates are treated with a reducing agent, DTT. In most experiments, we use a V5 mAb to probe for the V5 epitope attached to the carboxyl ends of Q1 constructs, although the C-20 Q1 pAb (Santa Cruz Biotechnology, Inc.) detects the same banding pattern as V5 mAb.

Fig. 4 A, top, depicts an immunoblot of Q1. Q1(-Cys)-I145C expressed alone or coexpressed with E1 variants migrates as a major 60-kD band. When it is coexpressed with E1-G40C or E1-K41C, an extra prominent 80-kD band appears, sometimes accompanied by a weaker 75-kD band (see also Fig. 5). No such bands are seen when Q1(-Cys)-I145C is coexpressed with E1-WT, and only extremely faint bands are seen when Q1(-Cys)-I145C is coexpressed with E1-L42C or E1-E43C. The 80- and 75-kD band sizes are similar to the expected sizes of disulfide-linked Q1 and E1 complexes (Q1 ~60 kD, partially core-glycosylated and unglycosylated E1 ~20 and 15 kD, respectively, see Fig. 5). DTT treatment abolishes both 80- and 75-kD bands in the Q1(-Cys)-I145C/E1-G40C lane, but does not affect the band size of Q1(-Cys)-I145C expressed alone or with E1-WT (Fig. 4 B). The bottom panel of Fig. 4 A confirms good protein expression of all five E1 variants. Therefore, the lack of the 80- and 75-kD bands when Q1(-Cys)-I145C is coexpressed with E1-WT, E1-L42C, or E1-E43C is not due to failure of efficient

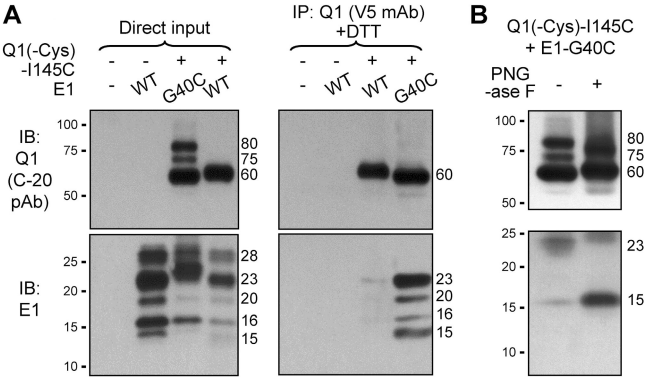

Figure 5. (A) Confirming the presence of E1 G40C in the 80- and 75-kD Q1-positive bands detected in whole cell lysate of COS-7 cells coexpressing Q1(-Cys)-I145C and E1-G40C. COS-7 cells are transfected with the cDNA(s) listed on top. An aliquot of the whole cell lysates is loaded onto the "direct input" lanes. The other aliquot is subjected to immunoprecipitation with V5 mAb. The immunoprecipitates are DTT treated and loaded onto the IP lanes. The Q1 and E1 are probed using a goat pAb against Q1 (C-20) and a rabbit pAb against E1. (B) Testing N-glycosylation in free E1 proteins and disulfide-linked Q1/E1 complex. Whole cell lysates from COS-7 cells coexpressing Q1(-Cys)-I145C and E1-G40C are treated with PNGase F or with buffer under the same conditions ("+" and "−" PNGase F) for 48 h at 37°C. The samples are fractionated by nonreducing SDS-PAGE and probed for Q1 and E1.

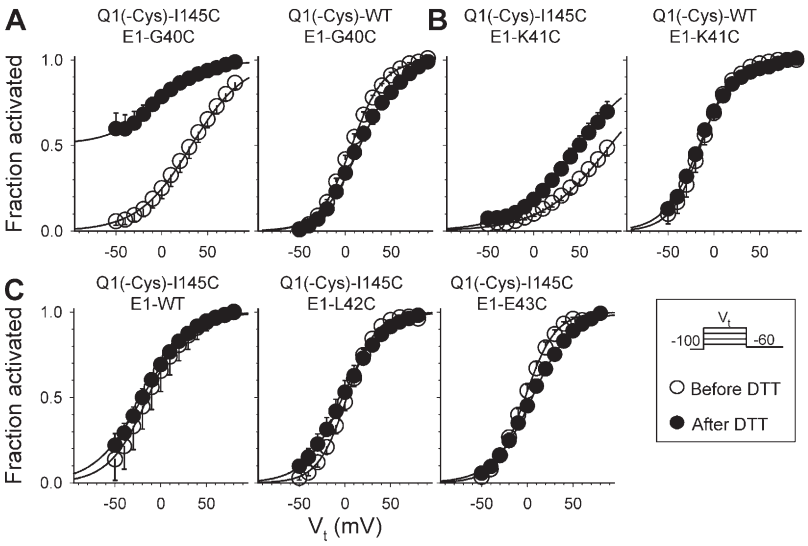

Figure 6. Effects of DTT treatment on the voltage dependence of activation of different combinations of Q1/E1 variants. The type of Q1 and E1 variants is marked on top of each panel: (A) E1-G40C coexpressed with Q1(-Cys)-I145C or Q1(-Cys)-WT, (B) E1-K41C coexpressed with Q1(-Cys)-I145C or Q1(-Cys)-WT, and (C) Q1(-Cys)-I145C coexpressed with E1-WT, E1-L42C, or E1-E43C. Voltage clamp protocol (diagrammed in the right bottom panel) and data analysis are the same as those described for Table I. The 2-s isochronal activation curves before and after DTT treatment are denoted by open and closed circles, respectively.

expression of these E1 variants. We propose that Cys introduced into Q1 position 145 can form disulfide bonds with Cys at E1 positions 40 and 41, but not at E1 position 42 or 43. The ratios of 80- to 60-kD band intensities are 0.30 ± 0.03 for Q1 145C/E1 40C (n = 21) and 0.12 ± 0.05 for Q1 145C/E1 41C (n = 4). It has been suggested that each Q1/E1 channel complex has two E1 subunits and four Q1 subunits (Chen et al., 2003a; Morin and Kobertz, 2008). If this is the case, the maximal degree of Q1 145C that can be disulfide linked to E1 40C is 50%, or the maximal ratio of 80 kD (or 80 + 75 kD, when the latter band is present) to 60-kD band intensities is 1.

Interestingly, although E1 migrates as multiple bands, there is only one major 80-kD band (sometimes accompanied by a 75-kD band) present in the Q1 immunoblot of Q1(-Cys)-I145C/E1-G40C or E1-K41C. In principle, we should be able to detect the E1 epitope in the 80- and 75-kD bands of proposed disulfide-linked Q1/E1 complexes using an antibody targeting the carboxyl terminus of E1 (e.g., pAb from Alomone). We have made several attempts using the Alomone E1 pAb to probe for E1-positive bands in the 80–75 kD range that are specific for Q1(-Cys)-I145C/E1-G40C and Q1(-Cys)-I145C/E1-K41C lanes. No, or only very faint, bands in the expected size range can be detected. It is possible that once E1 is associated with Q1, the epitope in its cytoplasmic domain is not accessible to, or cannot be recognized by, the E1 antibody. We use immunoprecipitation under strong denaturing, nonreducing conditions to test whether we can selectively coimmunoprecipitate E1-G40C with Q1(-Cys)-I145C, but not E1-WT with Q1(-Cys)-I145C (noncovalently associated, susceptible to denaturation-induced dissociation). The "direct input" lanes in Fig. 5 A confirm the presence of the 80- and 75-kD bands in the Q1(-Cys)-I145C/E1-G40C whole cell lysate. E1-WT expressed alone cannot be immunoprecipitated by the V5 mAb (second of IP lanes, Fig. 5 A), confirming the specificity of the immunoprecipitation reaction. Immunoprecipitate of Q1(-Cys)-I145C/E1-WT manifests a strong Q1 band but extremely faint E1 bands (top and bottom of the third IP lane, Fig. 5 A). This indicates efficient Q1 immunoprecipitation by the V5-mAb, but an almost total separation of noncovalently associated Q1(-Cys)-I145C and E1-WT by the strong denaturing conditions. However, DTT-treated immunoprecipitate of Q1(-Cys)-I145C/E1-G40C reveals strong E1 bands, accompanied by a strong 60-kD Q1 monomer band but a total disappearance of the 80- and 75-kD Q1 bands (bottom and top of the fourth IP lane, Fig. 5 A). These observations confirm the presence of E1 in the 80- and 75-kD Q1-positive bands in the whole cell lysate of Q1(-Cys)-I145C/E1-G40C.

The E1 immunoblot exhibits a complex banding pattern. In addition to the expected 15-kD unglycosylated E1 band, we see E1 bands at 28, 23, 20, and 16 kD (although there are variations in the relative band intensities among E1 WT and mutants, and among different batches of COS-7 cells). To test whether these higher molecular weight E1 bands are due to different degrees of glycosylation, and to further test whether the 80- and 75-kD bands detected in Q1 immunoblot (that we propose to represent disulfide-linked Q1/E1 complexes) contain glycosylated E1, we incubate whole cell lysate of Q1(-Cys)-I145C/E1-G40C with PNGase F for 24 or 48 h. We use such long incubation times to ensure as complete deglycosylation as possible under our experimental conditions (see Materials and methods). The control sample is incubated under the same conditions without PNGase F. Results of the 24-h and 48-h treatments are the same, indicating that the degree of deglycosylation has reached a plateau by 24 h. The latter data are shown in Fig. 5 B. PNGase F treatment should deglycosylate both core-glycosylated proteins (occurring in the endoplasmic reticulum) and complex glycosylated proteins

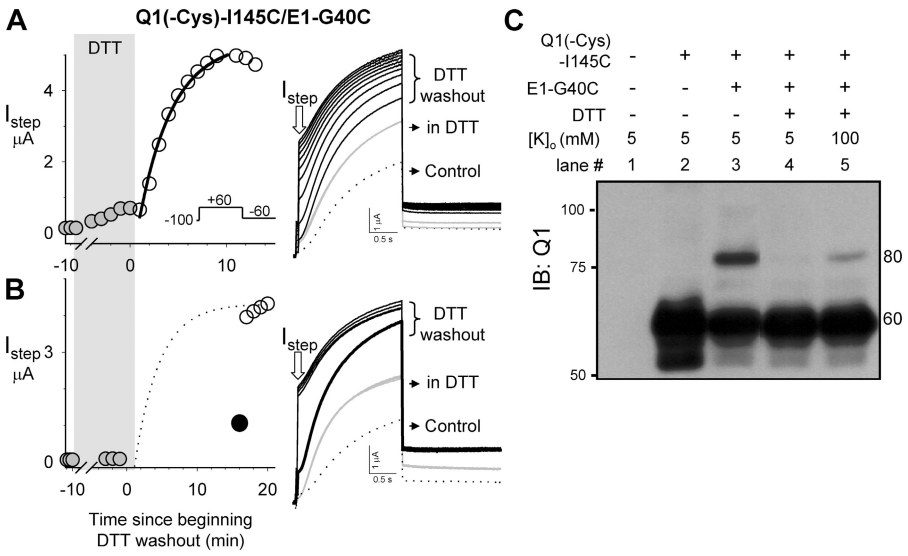

Figure 7. (A and B) Testing the state dependence of appearance of a constitutive component in oocytes expressing Q1(-Cys)-I145C/E1-G40C after DTT washout. Data from two experiments are shown, with time courses of appearance of the constitutive component (I_{step}) shown on the left, and superimposed current traces shown on the right. In both experiments, before DTT treatment, the oocytes manifest slowly activating currents without any constitutive component (dotted traces in right panels). The oocytes are exposed to DTT 10 mM for 10 min (gray shade, time axis breaks between start of DTT application and last few data points in DTT). In the presence of DTT, the current amplitudes increase but the currents remain slowly activating without a significant constitutive component (gray traces in the right panels). In A, during DTT washout the oocyte is repetitively pulsed from V_h −100 to +60 mV for 2 s, followed by a step to −60 mV for 2 s, once every minute (voltage clamp diagram in inset). The appearance of I_{step} follows a single exponential time course, with a time constant of 3.1 min (black thick curve superimposed on the open circle data points). In B, during DTT washout the oocyte is held at V_h −100 mV without pulsing for 15 min. The current induced by the first pulse after resuming pulsing is highlighted by the thick black current trace (right) and the small I_{step} component during the first pulse is highlighted by a solid black circle (left). The dotted curve is a scaled single exponential time course similar to that shown in Fig. 7 A. (C) Testing whether membrane depolarization by elevating $[K]_o$ facilitates disulfide bond formation between Q1 145C and E1 40C. COS-7 cells are transfected with cDNA(s) listed on the top two rows. Cells are incubated in medium containing 5 mM $[K]_o$ for 48 h. Cells in lanes 4 and 5 are treated with 10 mM DTT for 10 min to break disulfide bonds, followed by thorough rinsing to remove DTT. Cells in lane 4 are incubated in 5 mM $[K]_o$ medium, while cells in lane 5 are incubated in 100 mM $[K]_o$ medium for 10 min. All cell preparations are treated with NEM to protect free thiol groups, followed by whole cell lysis. Whole cell lysates are run on nonreducing SDS gel and probed for Q1 with V5 mAb.

(occurring in the Golgi apparatus) (Helenius and Aebi, 2001). PNGase F treatment does not shift the 60-kD Q1 monomer band (top, Fig. 5 B), indicating that the predicted N-glycosylation site in Q1 (N289, in the extracellular S5-P linker) is not glycosylated in the COS-7 cells. PNGase F treatment collapses the 80-kD band into the 75-kD band, suggesting that the former contains glycosylated E1 while the latter contains unglycosylated E1. In the E1 immunoblot (bottom, Fig. 5 B), PNGase F treatment produces a major 15-kD band, confirming that this represents unglycosylated E1.

Probing the Impact of Disulfide Bond Formation between Q1 145C and E1 40C or 41C on the Q1/E1 Channel Function

The above experiments show that disulfide bonds can be formed spontaneously between Q1 145C and E1 40C or E1 41C. The functional consequences of disulfide linkage between these Cys side chains may reveal the role of such Q1/E1 interactions in the I_{Ks} channel function. To address this issue, we use voltage clamp experiments on oocytes to study the effects of DTT treatment on the channel function of Q1(-Cys)-I145C/E1-G40C and Q1(-Cys)-I145C/E1-K41C.

Before DTT treatment, Q1(-Cys)-I145C/E1-G40C manifests a slowly activating current with $V_{0.5}$ of activation at 32.3 ± 4.0 mV and equivalent gating charge (z_g) of 0.88 ± 0.05 (Table I). There is no constitutive component even after a 30-min application of regular depolarizing pulses to +60 mV for 2 s once every min. After DTT treatment, an instantaneous current component appears, so that the activation curve has two components: a constitutive component of 42.3 ± 7.3% and a time-dependent component with $V_{0.5}$ of 2.1 ± 6.3 mV and z_g of 0.95 ± 0.11 (Fig. 6 A, left). Without DTT treatment, the Q1(-Cys)-I145C/E1-K41C channel manifests an extremely positively shifted activation curve. DTT treatment shifts the activation curve in the negative direction ($V_{0.5}$ 80.2 ± 5.7 and 55.0 ± 5.8 mV, before and after DTT, Fig. 6 B, left). On the other hand, DTT treatment has little or no effects on the following control cases: (a) only one Cys side chain present, Q1(-Cys)-WT/E1-G40C (Fig. 6 A, right), Q1(-Cys)-WT/E1-K41C (Fig. 6 B, right), and Q1(-Cys)-I145C/E1-WT (Fig. 6 C, left), and (b) known not capable of forming disulfide bonds, Q1(-Cys)-I145C/E1-L42C and Q1(-Cys)-I145C/E1-E43C (Fig. 6 C, middle and right). Therefore, the immunoblot data in COS-7 experiments and the voltage clamp data in oocyte experiments support each other. We conclude that the observed effects of DTT treatment on the activation curves of Q1(-Cys)-I145C/E1-G40C and Q1(-Cys)-I145C/E1-K41C can be attributed to a specific perturbation of disulfide bonds between these introduced Cys side chains.

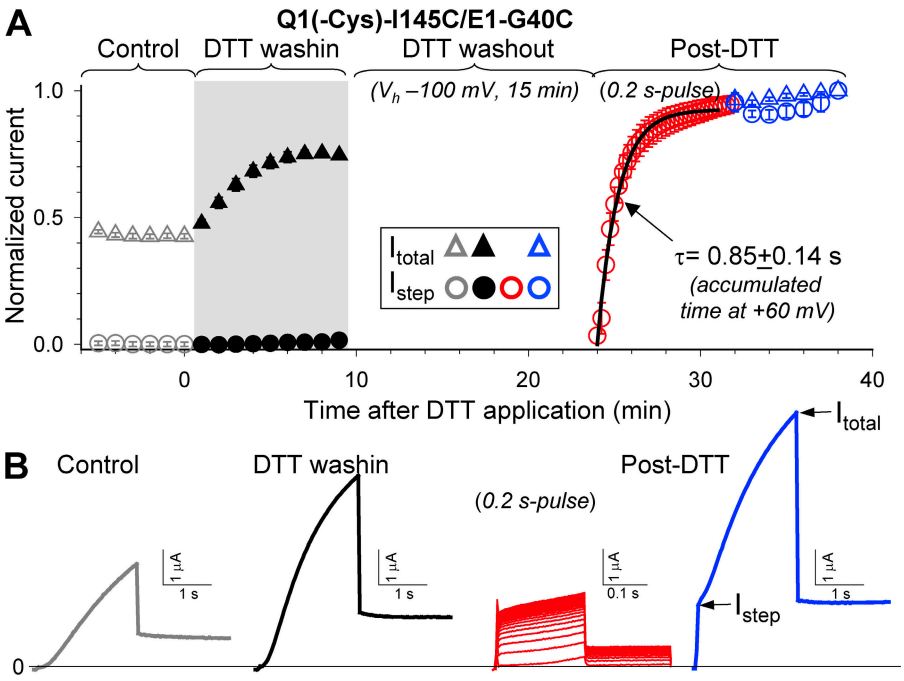

Figure 8. Estimating the rate of disulfide bond formation between Q1 I145C and E1 40C after DTT treatment. The experiment is divided into four phases. During the control and DTT (10 mM) washin phases, the membrane voltage is stepped from V_h −100 to +60 mV for 2 s and then to −60 mV for 2 s once every 60 s. The current amplitude at the beginning and end of the step to +60 mV (I_{step} and I_{total}, respectively) are monitored. After the DTT effects reach a steady state, the DTT washout phase begins during which the membrane is held at −100 mV for 15 min without depolarizing pulses. Then the 'post-DTT' phase begins that consists of two parts. During the first part, short (0.2 s) pulses to +60 mV applied once every 15 s are used to monitor the development of the constitutive component as indicated by the increase in I_{step}. Once the constitutive component reaches a steady state, the voltage clamp protocol is switched back to the 2-s depolarization pulses applied once every 60 s (as described above) to monitor the stability of I_{total} and I_{step}. (A) Average time course of changes in I_{total} and I_{step}. Data are pooled from four experiments. In each experiment, the amplitudes of I_{total} and I_{step} are normalized by their final values at the end of the experiment to allow data averaging. The black curve superimposed on data points obtained during the post-DTT 0.2-s pulse period represents an exponential fit to the time course of development of the constitutive component. The time constants are converted to cumulative depolarization time at +60 mV (0.85 ± 0.14 s, $n = 4$). (B) Original current traces from one representative experiment. Note the change in time calibration for the 0.2-s pulse current traces. The horizontal line denotes zero current level.

Testing the State Dependence and Rate of Disulfide Bond Formation between Q1 145C and E1 40C

As stated above, oocytes expressing Q1(-Cys)-I145C/E1-G40C without any DTT treatment exhibit a stable phenotype of slowly activating currents without any instantaneous current component. Exposing the oocytes to DTT induces a gradual increase in the current amplitudes. However, in the presence of DTT the current kinetics remains the same, i.e., slow activation without any instantaneous component (gray current traces in right panels of Fig. 7, A and B). In the experiment shown in Fig. 7 A, during DTT washout the oocyte membrane is depolarized to +60 mV for 2 s once every 60 s (diagram in the inset), i.e., the Q1(-Cys)-I145C/E1-G40C channels are repetitively activated. There is a further increase in the total current amplitude. More importantly, an instantaneous current component gradually develops. The time course of development of this instantaneous current component can be described by a single exponential function, with a τ value of 3.1 min (thick black curve superimposed on open circle data points in the left panel of Fig. 7 A). In the experiment shown in Fig. 7 B, during DTT washout, the oocyte membrane is held at −100 mV, i.e., the Q1(-Cys)-I145C/E1-G40C channels are maintained in the resting state. After thoroughly removing DTT from the bath, pulsing is resumed. The first pulse induces a slowly activating current with a very little instantaneous component (the thick black current trace in the right panel, and the large black data point in the left panel of Fig. 7 B). However, a prominent instantaneous current component develops during the second pulse and remains relatively stable during the following pulses. The dotted curve in the left panel of Fig. 7 B represents the expected time course of development of the instantaneous current component if the oocyte membrane was pulsed during DTT washout. Similar observations are obtained in four other experiments (three using the Fig. 7 B protocol, and one using the Fig. 7 A protocol with τ = 4.3 min). Therefore, after DTT treatment the Q1(-Cys)-I145C/E1-G40C channel can develop an instantaneous component only after the channel has been activated.

We use COS-7 expression and immunoblotting experiment to test whether disulfide bond formation between Q1 145C and E1 40C after DTT washout can also be facilitated by channel activation. Fig. 7 C, lane 3, shows the 80-kD band in cells coexpressing Q1(-Cys)-I145C and E1-G40C. Treating the COS-7 cells with 10 mM DTT for 10 min, followed by DTT washout for 10 min using the regular medium (containing 5 mM $[K]_o$), results in a total disappearance of the 80-kD band (lane 4). However, when the $[K]_o$ in the washing medium is elevated to 100 mM, and thus the COS-7 cell membrane is depolarized to ∼0 mV for 10 min during the washout

period, a faint but definite 80-kD band reappears (lane 5). Taken together, these data indicate that after DTT washout, 145C on Q1 and 40C on E1 can form a disulfide bond in the activated state of the channel, reaching nearly a steady state during a 2-s step to +60 mV. Disulfide bond formation between Q1 145C and E1 40C stabilizes the Q1(-Cys)-I145C/E1-G40C channel complex in a constitutively active state, creating the instantaneous current component.

The τ value of 3–4 min for the development of the instantaneous component in Q1(-Cys)-I145C/E1-G40C shown in Fig. 7 A represents the time required to clear DTT from the bath solution and to allow disulfide bond formation between Q1 145C and E1 40C. To more accurately estimate the rate of disulfide bond formation between Q1 145C and E1 40C, we design the experiments shown in Fig. 8. After thoroughly removing DTT from the bath solution while preventing disulfide bond formation by holding the membrane at −100 mV for 15 min, the membrane is stepped to +60 mV for 0.2 s once every 15 s. A constitutive component (I_{step}) gradually develops. The time course of growth of I_{step} is fit with a single-exponential function. The time constant is converted to the cumulative channel activation time at +60 mV, generating a τ value of 0.85 ± 0.14 s for disulfide bond formation between Q1 145C and E1 40C in the active state (Fig. 8 A, $n = 4$).

Testing the State Dependence and Rate of Disulfide Bond Formation between Q1 145C and E1 41C

Data summarized in Table I show that when both Q1 position 145 and E1 position 41 are mutated to Cys, the Q1/E1 channel complex is uniquely stabilized in the resting state. One possibility is that disulfide bond formation between Q1 145C and E1 41C stabilizes the Q1/E1 channel complex in the resting state. If so, reducing the disulfide bond by DTT treatment should make the channel more willing to activate. Indeed, Fig. 6 B shows that DTT treatment causes a negative shift in the voltage dependence of activation of Q1(-Cys)-I145C/E1-K41C.

We design the experiment shown in Fig. 9 A to estimate the rate of disulfide bond formation between Q1 145C and E1 41C. The current amplitude is monitored by activating the channels with 2-s depolarizing pulses to +60 mV once every 60 s. DTT application induces a gradual increase in the current amplitude, consistent with an increase in the channel open probability secondary to a reduction of disulfide bonds between Q1 145C and E1 41C. Upon DTT washout, the current amplitude gradually declines. The time course of current reduction is much slower than that of DTT clearance from the bath solution (Fig. 9 B). This decline in current amplitude after DTT removal is consistent with a reformation of disulfide bonds between Q1 145C and E1 41C, which stabilize the channels in the resting state and reduce the channel open probability. This time

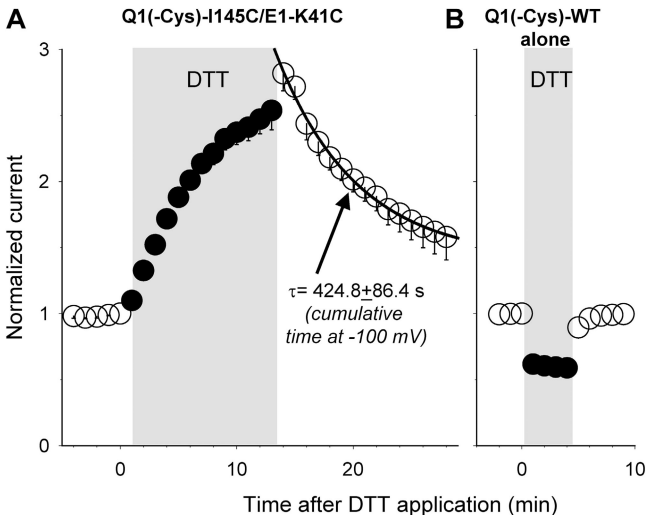

Figure 9. (A) Time course of changes in current amplitudes of Q1(-Cys)-I145C/E1-K41C before, during, and after DTT (10 mM) exposure. Data are averaged from six experiments. Oocyte membrane is pulsed from V_h −100 mV to +60 mV for 2 s, followed by repolarization to −60 mV for 2 s, once every 60 s. Current amplitudes at the end of the +60-mV step is measured and normalized by the control current before DTT exposure. The duration of DTT exposure is denoted by gray shade. The time course of current reduction after DTT washout is fit with a single exponential function (smooth curve superimposed on data points after DTT). The time constant (τ) is converted to cumulative time at V_h −100 mV (when channels are in the resting state). Mean and SEM values of τ are listed in inset. (B) Time course of changes in current amplitude of Q1(-Cys)-WT expressed alone before, during (gray shade), and after exposure to 10 mM DTT. Since there is no Cys in the Q1 channel, this experiment reveals a direct current-suppressing effect of DTT on the Q1 channel. The rapid onset of DTT effect and rapid/complete reversal reflect the time course of DTT equilibration in the bath solution during wash-in and rate of DTT clearance during washout.

course can be well described by a single exponential function. The time constant is converted to cumulative time at −100 mV, when the Q1(-Cys)-I145C/E1-K41C channels are in the resting state. This gives an estimated τ value for disulfide bond formation between Q1 145C and E1 41C in the resting state of 425 ± 86 s ($n = 6$). The slower rate of disulfide bond formation between Q1 145C and E1 41C, relative to the rate of disulfide bond formation between Q1 145C and E1 40C (Fig. 8 A), is consistent with the weaker 80-kD band seen in immunoblots of Q1(-Cys)-I145C/E1-K41C relative to Q1(-Cys)-145C/E1-G40C (Fig. 4 A). These observations indicate that, although disulfide bonds can be formed in both Cys pairs, Q1 145C and E1 41C in the resting state are farther apart than the distance between Q1 145C and E1 40C in the activated state.

DISCUSSION

The major findings in this study can be summarized as the following. (a) Cys introduced into Q1 position 145

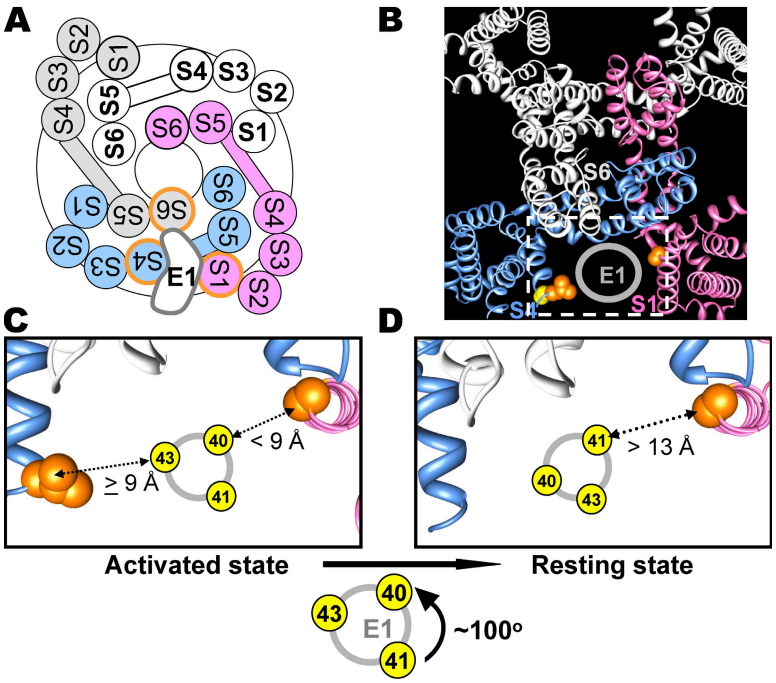

Figure 10. A structural model of E1 association with the Q1 channel, and dynamic interactions between the extracellular ends of their transmembrane domains. (A) Top view of the arrangement of transmembrane segments in a tetrameric Q1 channel based on the crystal structure of Kv1.2 (2A79.pdb). The four Q1 subunits are color coded light blue, pink, white, and light gray. S1–S4 of the voltage-sensing domains (VSDs), S5–S6 of the pore domains (PDs), and the S4–S5 linkers (rectangles connecting S4 and S5) are marked. The E1 transmembrane domain is in a putative "KCNE-binding pocket," where E1 makes contacts with S4, S6, and S1 of three separate Q1 subunits. (B) Top view of a tetrameric Kv1.2 structure (using the 2A79.pdb coordinates), color coded in the same manner as in A. L290 at the extracellular end of S4 of the light blue subunit and UNK50 at the extracellular end of S1 of the pink subunit that serve as surrogates for A226 and I145 in Q1, respectively, are highlighted by the orange space-filled model. A291 at the extracellular end of S4 in the light blue Q1 subunit is also shown as yellow space-filled model. S6 of the light gray subunit is marked. The E1 transmembrane domain is signified by the open gray circle. The close-up view of the region demarcated by white dashed lines is shown in C and D. (C) In the activated state of the Q1/E1 channel complex, the E1 helix is oriented in such a manner that E1 position 40 faces toward Q1 position 145 (UNK50 in 2A79), and E1 position 43 faces toward Q1 position 226 of the adjacent subunit (L290 in 2A79). (D) Upon channel deactivation, the E1 helix is postulated to rotate ~100° counterclockwise so that in the resting state E1 position 41 faces toward Q1 position 145. In C and D, the C_β–C_β distances are deduced by the rates of disulfide formation (Fig. 8 A and Fig. 9 A) (Nakajo and Kubo, 2007) and the experimentally determined relationship between the rate of disulfide formation and the distance between surface Cys pair (Careaga and Falke, 1992) (more in text).

can form a disulfide bond with Cys introduced into E1 positions 40 and 41, but not Cys introduced into E1 position 42 or 43. (b) Q1(-Cys)-I145C/E1-G40C exhibits a constitutive component after DTT treatment. This constitutive component can be attributed to disulfide bond formation between Q1 145C and E1 40C when the channel reaches the activated state, which then stabilizes the channel in the activated state. (c) Q1(-Cys)-145C/E1-K41C exhibits an extremely positive voltage range of activation, and DTT treatment shifts the activation curve in the negative direction. No such effect of DTT is observed with Q1(-Cys)-I145C/E1-WT or Q1(-Cys)-WT/E1-K41C. These observations indicate that Q1 145C and E1 41C can form a disulfide bond in the resting state, which further stabilizes the channel in the resting state.

A Structural Model for the KCNQ1/KCNE1 Channel Complex

A model of the Q1/E1 channel complex needs to account for the following observations: (a) E1 mid-TMD region interacts with Q1 mid-S6 region, likely E1 position 58 interacting with Q1 position 338 and E1 positions 54/55 interacting with Q1 position 331 (Tapper and George, 2001; Melman et al., 2004; Panaghie et al., 2006), (b) E1 position 43 comes very close to Q1 position 226 (extracellular end of S4) in the activated state so that cysteine side chains engineered into these positions can form a disulfide bond (Nakajo and Kubo, 2007), and (c) E1 positions 40 and 41 come very close to Q1 position 145 in the activated and resting states, respectively, so that Cys side chains engineered into these positions can form disulfide bonds. We propose that E1 binds in a "KCNE binding pocket" between VSDs of two adjacent Q1 subunits, and juxtaposed to the pore domain (PD) of a third Q1 subunit. Fig. 10 A depicts a schematic top view of our model, with the four Q1 subunits color coded light blue, pink, white, and light gray. The arrangement of S1–S4 in the VSD, the arrangement of S5–S6 in the PD, and the relationship between VSD and PD of the same subunit are based on the crystal structure of Kv1.2 (2A79.pdb). E1 is making contact with S1, S4, and S6 from three different Q1 subunits.

Dynamic Interaction between the Extracellular End of KCNE1 and KCNQ1

To estimate the peptide backbone mobility involved in disulfide bond formation in a functional protein, ideally one wants to start with a high-resolution crystal structure of the protein to estimate the C_β–C_β distance between the two positions of interest (where engineered Cys side chains can form a disulfide bond). One can then deduce how much translational, rotational, and/or tilting movement of the peptide backbone is necessary to bring the

C_β–C_β distance between the two Cys side chains to within 4.6 Å so that they can form a disulfide. In our case, we use the Kv1.2 crystal structure as an approximation of the Q1 channel. In the 2A79 structure, the S1 helix is simulated by a poly-Ala chain, and there is no S1–S2 linker structure. Furthermore, Kv1.2 and Q1 are quite divergent in their S1 helix and S1–S2 linker sequences. Therefore, there is no ready way to assign a "145-equivalent" position in the 2A79 structure. We use UNK50 in chain C of 2A79 (simulating the T1–S1 linker and the S1 helix) as a surrogate for position 145 in Q1. UNK50 is the outer most position of the simulated S1 in 2A79, facing toward the space where we postulate the associated E1 is located, the "KCNE binding pocket" (Fig. 10 B). A226 of Q1 is equivalent to A291 of Kv1.2. In the 2A79 structure, the A291 side chain faces away from the KCNE binding pocket. On the other hand, its next neighbor L290 faces toward the KCNE binding pocket. Since it has been suggested that S4 helix rotates in response to changes in the transmembrane voltage (Gandhi et al., 2003), it is reasonable to assume that both L290 and A291 have a chance to face toward the KCNE binding pocket during channel activation gating transitions. Therefore, we use L290 as a surrogate for position 226 in Q1. Fig. 10 B depicts a top view of a 2A79 tetramer structure. UNK50 at the extracellular end of S1 in one (pink) subunit and L290 at the extracellular end of S4 in the adjacent (light-blue) subunit are highlighted by the orange space-filled model. A291 is also shown (yellow space-filled model). S6 of a third (light-gray) subunit is marked, and the location of the putative E1 TMD is denoted by an open gray circle.

To simulate the experimental findings that in the activated state, E1 40C can form a disulfide bond with Q1 145C while E1 43C can form a disulfide bond with Q1 226C (Nakajo and Kubo, 2007), we orient the E1 TM helix in such a way that E1 position 40 faces toward UNK50, and E1 position 43 faces toward L290 of an adjacent subunit. The rate of disulfide formation (K_{ss}) is determined by the rate of thiol side chain collisions (K_c) and an "efficiency factor" (σ): $K_{ss} = \sigma K_c$ (Careaga and Falke, 1992). The efficiency factor varies with the environment, but should be similar for thiol side chains in a similar environment. K_c is determined by the distance between thiol side chains and the flexibility of peptide backbone(s) harboring them. Cys pairs were engineered into surface α helices of D-galactose chemosensory receptor of *Escherichia coli*, whose high-resolution crystal structure was available, and the rates of disulfide formation between these Cys pairs were determined. It was found that the K_{ss} value decreased as the C_β–C_β distance between the Cys pair increased (Careaga and Falke, 1992). Assuming that the efficiency factor for Cys pairs studied here (on the extracellular surface of the Q1/E1 channel complex) is similar to that of surface Cys pairs in D-galactose chemosensory receptor, we use the above experimentally determined relationship between K_{ss} and C_β–C_β distance to deduce the distance between the Cys pairs studied here. The time constant of disulfide bond formation between E1 40C and Q1 145C in the activated state is ~1 s (Fig. 8 A). Assuming that disulfide formation is a first-order reaction, this translates into a rate of ~1 s^{-1}, placing the C_β–C_β distance between E1 40C and Q1 145C at <9 Å (Fig. 10 C). The rate of disulfide bond formation between E1 43C and Q1 226C in the activated state is estimated to be ~0.1 s^{-1} (Nakajo and Kubo, 2007), placing the C_β–C_β distance between these two positions at ≥9 Å. To account for the observation that in the resting state, E1 41C can form a disulfide bond with Q1 145C, we rotate the E1 TM helix counterclockwise by ~100°, so that E1 position 41 faces toward UNK50 (Fig. 10 D). The time constant of disulfide formation between Q1 145C and E1 41C in the resting state is ~425 s. This translates into a rate of ~2.5 ms^{-1}, placing the C_β–C_β distance between E1 41C and Q1 145C at >13 Å (Fig. 10 D).

A new concept emerging from this model is that E1 is not a stationary, passive partner of the Q1 channel. Instead, E1 can engage in I_{Ks} gating in a more dynamic fashion. Is there any reason to believe that E1 can engage in molecular motions during activation gating transitions of the Q1/E1 channel complex? In response to changes in the transmembrane voltage, the voltage sensor S4 may rotate, translate, and change its tilt angle (Gandhi et al., 2003; Starace and Bezanilla, 2004). The S4 movement is transmitted to the S6 helix (Long et al., 2005b), whose hinge points then move to open the "activation gate" (cytoplasmic halves of the S6 helices) (Hackos et al., 2002; Seebohm et al., 2006). Through the contacts between S4 and/or S6 with E1, the molecular motions of S4 and S6 can be transmitted to the E1 TM helix, causing it to engage in molecular motions. Therefore, based on the experimental findings and the Kv1.2 crystal structure, we propose that the extracellular end of E1 TM helix may "wobble" between the voltage-sensing domains of two adjacent Q1 subunits, allowing E1 positions 40 and 43 to come close to Q1 positions 145 and 226, respectively. Furthermore, the E1 TM helix may rotate during gating transitions, allowing E1 positions 40 and 41 to come close to the same Q1 position 145 in a gating state-dependent manner. It is equally possible that there is little or no molecular motion in E1 during I_{Ks} gating. Instead, it is the molecular motions of the S1 and/or S4 segments in Q1 that create the state-dependent disulfide bond formation observed here and by others (Nakajo and Kubo, 2007). A definite distinction between these possibilities probably has to wait till there is a comprehensive map of contact points between Q1 and E1, knowledge of the gating state dependencies of these contacts, and the ability to perform molecular dynamics simulations of the Q1/E1 channel complex in a time scale relevant for the I_{Ks} gating kinetics.

Requirement for DTT Treatment to Reveal Disulfide Bond Formation between Q1 145C and E1 40C

There is no straightforward explanation for why we need to treat oocytes expressing Q1-I145C/E1-G40C with DTT, and then wash out DTT, to reveal the functional consequence of disulfide linkage between the two engineered Cys side chains. We suspect that without DTT treatment, E1 40C may form a disulfide bond with something other than Q1 145C, thus preventing disulfide formation between the two and the occurrence of the instantaneous current component. The total current amplitude is also relatively small. DTT treatment breaks the disulfide bond between E1 40C and the unidentified protein. Perhaps this allows a reorientation of the E1 40C or even a larger scale motion of the E1 peptide. This leads to a prominent increase in the total current amplitude, and upon DTT washout, disulfide bond formation between E1 40C and Q1 145C and the appearance of the constitutive current component. Our suspicion comes from indirect evidence. In E1 immunoblots we often observe a strong 40-kD band in Cys-substituted E1 mutants but not in E1-WT, and DTT treatment abolishes the 40-kD band.

This work was supported by HL46451 and HL67840 from National Heart, Lung, and Blood Institute, National Institutes of Health (to G.N. Tseng).

Olaf S. Andersen served as editor.

Submitted: 29 January 2008
Accepted: 2 May 2008

REFERENCES

Abbott, G.W., and S.A.N. Goldstein. 1998. A superfamily of small potassium channel subunits: form and function of the MinK-related peptides (MiRPs). *Q. Rev. Biophys.* 31:357–398.

Abitbol, I., A. Peretz, C. Lerche, A.E. Busch, and B. Attali. 1999. Stilbenes and fenamates rescue the loss of I_{Ks} channel function induced by an LQT5 mutation and other IsK mutants. *EMBO J.* 18:4137–4148.

Aggeli, A., M.L. Bannister, M. Bell, N. Boden, J.B.C. Findlay, M. Hunter, P.F. Knowles, and J.-C. Yang. 1998. Conformation and ion-channeling activity of a 27-residue peptide modeled on the single-transmembrane segment of the IsK (minK) protein. *Biochemistry.* 37:8121–8131.

Barhanin, J., F. Lesage, E. Guillemare, M. Fink, M. Lazdunski, and G. Romey. 1996. KvLQT1 and IsK (minK) proteins associate to form the I_{Ks} cardiac potassium current. *Nature.* 384:78–80.

Careaga, C.L., and J.J. Falke. 1992. Thermal motions of surface α-helices in the D-galactose chemosensory receptor. Detection by disulfide trapping. *J. Mol. Biol.* 226:1219–1235.

Chen, H., and S.A.N. Goldstein. 2007. Serial perturbation of MinK in I_{Ks} implies an α-helical transmembrane span traversing the channel corpus. *Biophys. J.* 93:2332–2340.

Chen, H., L.A. Kim, S. Rajan, S. Xu, and S.A.N. Goldstein. 2003a. Charybdotoxin binding in the I_{Ks} pore demonstrates two minK subunits in each channel complex. *Neuron.* 40:15–23.

Chen, Y.-H., S.-J. Xu, S. Bendahhou, X.-L. Wang, Y. Wang, W.-Y. Xu, H.-W. Jin, H. Sun, X.-Y. Su, Q.-N. Zhuang, et al. 2003b. KCNQ1 gain-of-function mutation in familial atrial fibrillation. *Science.* 299:251–254.

Gandhi, C.S., E. Clark, E. Loots, A. Pralle, and E.Y. Isacoff. 2003. The orientation and molecular movement of a K^+ channel voltage-sensing domain. *Neuron.* 40:515–525.

Goldstein, S.A.N., and C. Miller. 1991. Site-specific mutations in a minimal voltage-dependent K^+ channel alter ion selectivity and open-channel block. *Neuron.* 7:403–408.

Hackos, D.H., T.-H. Chang, and K.J. Swartz. 2002. Scanning the intracellular S6 activation gate in the Shaker K^+ channel. *J. Gen. Physiol.* 119:521–531.

Helenius, A., and M. Aebi. 2001. Intracellular functions of N-linked glycans. *Science.* 291:2364–2369.

Hong, K., D.R. Piper, A. Diaz-Valdecantos, J. Brugada, A. Oliva, E. Burashnikov, J. Santos-de-Soto, J. Grueso-Montero, E. Diaz-Enfante, P. Brugada, et al. 2005. De novo KCNQ1 mutation responsible for atrial fibrillation and short QT syndrome in utero. *Cardiovasc. Res.* 68:433–440.

Jost, N., L. Virag, M. Bitay, J. Takacs, C. Lengyel, P. Biliczki, Z. Nagy, G. Bogats, D.A. Lathrop, J.G. Papp, and A. Varro. 2005. Restricting excessive cardiac action potential and QT prolongation. A vital role for I_{Ks} in human ventricular muscle. *Circulation.* 112:1392–1399.

Jespersen, T., M. Grunnet, and S.-P. Olesen. 2005. The KCNQ1 potassium channel: from gene to physiological function. *Physiology (Bethesda).* 20:408–416.

Li, G.-R., J. Feng, L. Yue, M. Carrier, and S. Nattel. 1996. Evidence for two components of delayed rectifier K^+ current in human ventricular myocytes. *Circ. Res.* 78:689–696.

Liu, W.L., D.Y. Hu, P. Li, C.L. Li, X.G. Qin, Y.T. Li, L. Li, Z.M. Li, W. Dong, Y. Qi, and Q. Wang. 2006. Novel mutations of potassium channel KCNQ1 S143L and KCNH2 Y475C genes in Chinese pedigrees of long QT syndrome. *Zhonghua Nei Ke Za Zhi.* 45:463–466.

Liu, Y., and R.H. Joho. 1998. A side chain in S6 influences both open-state stability and ion permeation in a voltage-gated K^+ channel. *Pflugers Arch.* 435:654–661.

Long, S.B., E.B. Campbell, and R. MacKinnon. 2005a. Crystal structure of a mammalian voltage-dependent *Shaker* family K^+ channel. *Science.* 309:897–903.

Long, S.B., E.B. Campbell, and R. MacKinnon. 2005b. Voltage sensor of Kv1.2: structural basis of electromechanical coupling. *Science.* 309:903–908.

Lundby, A., L.S. Raven, J.H. Svendsen, S.-P. Olesen, and N. Schmitt. 2007. KCNQ1 mutation Q147R is associated with atrial fibrillation and prolonged QT-interval. *Heart Rhythm.* 4:1532–1541.

Melman, Y.F., A. Krumerman, and T.V. McDonald. 2002. A single transmembrane site in the KCNE-encoded proteins controls the specificity of KvLQT1 channel gating. *J. Biol. Chem.* 277:25187–25194.

Melman, Y.F., S.Y. Um, A. Krumerman, A. Kagan, and T.V. McDonald. 2004. KCNE1 binds to the KCNQ1 pore to regulate potassium channel activity. *Neuron.* 42:927–937.

Morin, T.J., and W.R. Kobertz. 2007. A derivatized scorpion toxin reveals the functional output of heteromeric KCNQ1-KCNE K^+ channel complexes. *ACS Chem. Biol.* 2:469–473.

Morin, T.J., and W.R. Kobertz. 2008. Counting membrane-embedded KCNE β-subunits in functioning K^+ channel complexes. *Proc. Natl. Acad. Sci. USA.* 105:1478–1482.

Nakajo, K., and Y. Kubo. 2007. KCNE1 and KCNE3 stabilize and/or slow voltage sensing S4 segment of KCNQ1 channel. *J. Gen. Physiol.* 130:269–281.

Napolitano, C., S.G. Priori, P.J. Schwartz, R. Bloise, E. Ronchetti, J. Nastoli, G. Bottelli, M. Cerrone, and S. Leonardi. 2005. Genetic testing in the long QT syndrome. Development and validation of an efficient approach to genotyping in clinical practice. *JAMA.* 294:2975–2980.

Panaghie, G., and G.W. Abbott. 2007. The role of S4 changes in voltage-dependent and voltage-independent KCNQ1 potassium channel complexes. *J. Gen. Physiol.* 129:121–133.

Panaghie, G., K.K. Tai, and G.W. Abbott. 2006. Interaction of KCNE subunits with the KCNQ1 K^+ channel pore. *J. Physiol.* 570:455–467.

Sanguinetti, M.C., M.E. Curran, A. Zou, J. Shen, P.S. Spector, D.L. Atkinson, and M.T. Keating. 1996. Coassembly of KvLQT1 and minK (IsK) proteins to form cardiac I_{Ks} potassium channel. *Nature.* 384:80–83.

Schreibmayer, W., H.A. Lester, and N. Dascal. 1994. Voltage clamping of *Xenopus laevis* oocytes utilizing agarose-cushion electrodes. *Pflugers Arch.* 426:453–458.

Seebohm, G., N. Strutz-Seebohm, O. Ureche, R. Baltaev, A. Lampert, G. Kornichuk, K. Kamiya, T.V. Wuttke, H. Lerche, M.C. Sanguinetti, and F. Lang. 2006. Differential roles of S6 domain hinges in the gating of KCNQ potassium channels. *Biophys. J.* 90:2235–2244.

Sesti, F., and S.A.N. Goldstein. 1998. Single-channel characteristics of wild-type I_{Ks} channels and channels formed with two minK mutants that cause long QT syndrome. *J. Gen. Physiol.* 112:651–663.

Starace, D.M., and F. Bezanilla. 2004. A proton pore in a potassium channel voltage sensor reveals a focused electric field. *Nature.* 427:548–553.

Tai, K.K., and S.A.N. Goldstein. 1998. The conduction pore of a cardiac potassium channel. *Nature.* 391:605–608.

Tapper, A.R., and A.L. George Jr. 2000. MinK subdomains that mediate modulation of and association with KvLQT1. *J. Gen. Physiol.* 116:379–390.

Tapper, A.R., and A.L. George Jr. 2001. Location and orientation of minK within the I_{Ks} potassium channel complex. *J. Biol. Chem.* 276:38249–38254.

Tian, C., C.G. Vanoye, C. Kang, R.C. Welch, H.J. Kim, A.L. Jr. George, and C.R. Sanders. 2007. Preparation, functional characterization, and NMR studies of human KCNE1, a voltage-gated potassium channel accessory subunit associated with deafness and long QT syndrome. *Biochemistry.* 46:11459–11472.

Tristani-Firouzi, M., and M.C. Sanguinetti. 1998. Voltage-dependent inactivation of the human K^+ channel KvLQT1 is eliminated by association with minimal K^+ channel (minK) subunits. *J. Physiol.* 510:37–45.

Tseng-Crank, J.C.L., G.-N. Tseng, A. Schwartz, and M.A. Tanouye. 1990. Molecular cloning and functional expression of a potassium channel cDNA isolated from a rat cardiac library. *FEBS Lett.* 268:63–68.

Wang, Z., B. Fermini, and S. Nattel. 1994. Rapid and slow components of delayed rectifier current in human atrial myocytes. *Cardiovasc. Res.* 28:1540–1546.

Wu, D.-M., M. Jiang, M. Zhang, X.-S. Liu, Y.V. Korolkova, and G.-N. Tseng. 2006a. KCNE2 is colocalized with KCNQ1 and KCNE1 in cardiac myocytes and may function as a negative modulator of I_{Ks} current amplitude in the heart. *Heart Rhythm.* 3:1469–1480.

Wu, D.-M., L.-P. Lai, M. Zhang, H.-L. Wang, M. Jiang, X.-S. Liu, and G.-N. Tseng. 2006b. Characterization of an LQT5-related mutation in KCNE1, Y81C: implications for a role of KCNE1 cytoplasmic domain in I_{Ks} channel function. *Heart Rhythm.* 3:1031–1040.

Zareba, W., A.J. Moss, G. Sheu, E.S. Kaufman, S.G. Priori, G.M. Vincent, J.A. Towbin, J. Benhorin, P.J. Schwartz, C. Napolitano, et al. 2003. Location of mutation in the KCNQ1 and phenotype presentation of long QT syndrome. *J. Cardiovasc. Electrophysiol.* 14:1149–1153.